General form for obtaining discrete orthogonal moments

H. Zhu[1]   M. Liu[2]   H. Shu[3]   H. Zhang[3]   L. Luo[3]

[1]Department of Electronics and Communications Engineering, East China University of Science and Technology, Shanghai 200237, People's Republic of China
[2]Centre for Networking and Telecommunications Research, School of Computing, Science and Engineering, University of Salford, Salford, UK
[3]Laboratory of Image Science and Technology, School of Computer Science and Engineering, Southeast University, Nanjing 210096, People's Republic of China
E-mail: shu.list@seu.edu.cn

Abstract: Discrete orthogonal moments such as Tchebichef moments and Krawtchouk moments are more powerful in image representation than traditional continuous orthogonal moments. However, less work has been done for the summarisation of these discrete orthogonal moments. This study proposes two general forms which will simplify and group the discrete orthogonal Tchebichef and Krawtchouk polynomials and their corresponding moments, and discusses their importance in theories and applications. Besides, the proposed general form can be used to obtain other three discrete orthogonal moments: Hahn moments, Charlier moments and Meixner moments. Computations of these discrete orthogonal polynomials are also discussed in this task, including the recurrence relation with respect to variable x and order n. Some properties of these discrete orthogonal moments, which are of particular value to image processing applications, such as energy compact capability and signal decorrelation, are also presented. Finally, the study evaluates these discrete orthogonal moments in terms of the capacity of image reconstruction and image compression, and discusses the importance of the proposed general form in theories and engineering.

1 Introduction

Moments and moment functions have been extensively used for feature extraction in pattern recognition and object classification [1, 2]. Moments with a continuous orthogonal base set, such as Legendre, Zernike, pseudo-Zernike and generalised pseudo-Zernike polynomials, can be used to represent an image with minimum redundancy information [3, 4]. However, the computation of these moments requires a coordinate transformation and a suitable approximation of the continuous moment's integrals, thus leading to further computational complexity and discretisation errors [5]. Recently, discrete orthogonal Tchebichef and Krawtchouk moments have been introduced to the field of image analysis [6, 7]. It was proved that these discrete orthogonal moments have better capability in image representation than the traditional continuous orthogonal moments. Taking a cue from their work, we recently

introduced the sets of Hahn (Hahn–Eberlein), Dual Hahn and Racah moment functions in succession [8–10]. We adopted a general form to define these moments. Among them, the Racah and Dual Hahn orthogonal polynomials used in Racah moments and Dual Hahn moments, respectively, are orthogonal on non-uniform lattice. The Hahn polynomials are orthogonal on the constant mesh. The use of discrete orthogonal polynomials as basis functions in image moments will eliminate the need for numerical approximation, and satisfy the orthogonal property precisely in a discrete domain as image coordinate space is a discrete domain [5, 6]. As it is well known, all these discrete orthogonal moments are adopting the classical orthogonal polynomials of one variable as basis functions. To the best of our knowledge until now, there is no such general form ever used to calculate all these discrete orthogonal polynomials that are used to define their corresponding discrete orthogonal moments.

335

The present studies will focus on the general form to summarise discrete orthogonal Tchebichef, Krawtchouk, Hahn, Meixner and Charlier moments (TM, KM, HM, MM and CM). Note that there are three commonly used standardisations in Hahn polynomials: $Q_n(x; a, b, N)$, $h_n^{(a,b)}(x, N)$ and Hahn–Eberlein polynomials $h_n^{(u,v)}(x, N)$ [11–13]. The first one and the last one were used to define Hahn moments by Yap *et al.* [14] and by our previous work [8], respectively. Their characteristics are listed in [15]. No reports about the second standardisation used in image analysis areas have been found. In this study, it is chosen to construct another new Hahn moments. Besides, two other discrete orthogonal moments, Meixner and Charlier moments are also introduced from the proposed general form.

Owing to very time-consuming of computing polynomials' values by using hypergeometric function and gamma function, the three-term recurrence relations of classical orthogonal polynomials are usually adopted to calculate the polynomial values. However, one problem encountered in the calculation of high-order polynomial values is the propagation of numerical errors while using the recursive formula with respect to order n. This error can have an exponential growth, thus severely affects the quality of image reconstruction. To remedy this problem, the modified recurrence relation for these discrete orthogonal polynomials is given in this study for decreasing the computational cost in the calculation of moments and improving the precision of image reconstruction. In addition, some useful properties of these discrete orthogonal moments are also discussed, such as signal decorrelation and energy compaction.

When the parameters of orthogonal polynomials are set as some special values, the emphasis region of these polynomials is completely different. Thus, some moments, such as Krawtchouk and Hahn moments, can be set on local feature extraction mode by using some special parameters, and Tchebichef, Meixner and Charlier moments are more focusing on the global feature extraction. By using such a method, the proposed 2-D moment functions are able to extract the features of any selected region-of-interest (ROI) by choosing appropriate parameters and have more flexibility in describing an image.

The main contribution of this study is to propose two general forms of recurrence relations with respect to variable x and order n for calculating the discrete orthogonal polynomials and moments. Then, this work defines three new discrete orthogonal moments (Hahn moments, Meixner moments and Charlier moments) by using the proposed general form. The energy compaction and signal decorrelation are also used to explain and compare the image compaction capabilities of discussed moments in theory.

This paper is structured as follows: In Section 2, we recall the definition of the classical discrete orthogonal polynomials with one variable. Two recurrence relations about these polynomials are given in Section 3. In Section 4, we define 1-D and 2-D discrete orthogonal moments. The properties of these discrete orthogonal moments and some experimental results are discussed in Section 5. Section 6 concludes the paper.

2 Classical discrete orthogonal polynomials of one variable

The classical discrete orthogonal polynomials with one variable will be used in this study, so we address them in this section. One can refer to [11, 12] for more details. The discrete orthogonal polynomials can be classified into two categories. One is the set of polynomials that are orthogonal on the uniform lattice $\{x = 0, 1, 2, \ldots\}$. The discrete Tchebichef, Krawtchouk, Hahn, Meixner and Charlier polynomials belong to this category. The other one consists of the polynomials being orthogonal on the non-uniform lattice $\{x = x(s), s = 0, 1, 2, \ldots\}$ [9–12]. In this study, we consider only the former set of polynomials. These discrete orthogonal polynomials are defined as the polynomial solutions of the following difference equation

$$\sigma(x)\Delta\nabla p_n(x) + \tau(x)\Delta p_n(x) + \lambda_n p_n(x) = 0 \qquad (1)$$

where $\Delta p_n(x) = p_n(x + 1) - p_n(x)$, $\nabla p_n(x) = p_n(x) - p_n(x - 1)$ denote the forward and backward finite difference operator, respectively. $\sigma(x)$ and $\tau(x)$ are the functions of second and first degree, respectively, λ_n is an appropriate constant. The solution of this partial difference equation can be expressed by Rodrigues formula as follows

$$p_n(x) = \frac{B_n}{w(x)} \nabla^n[w_n(x)] \qquad (2)$$

where $w(x)$ is the weight function $w_n(x)$ in the case of $n = 0$. Thus, the polynomials solutions of (1) are determined by (2) depending on the normalising factors B_n. For the backward difference operator ∇ we have the property [11, 12]

$$\nabla^n f(x) = \sum_{k=0}^{n} \binom{n}{k}(-1)^k f(x - k) \qquad (3)$$

Combining Rodrigues formula and (3), we can obtain an explicit expression for the polynomials $p_n(x)$.

The classical orthogonal polynomials with one discrete variable satisfy the following three-term recurrence relation

$$x p_n(x) = \alpha_n p_{n+1}(x) + \beta_n p_n(x) + \gamma_n p_{n-1}(x) \qquad (4)$$

The polynomials $p_n(x)$ satisfy an orthogonality relation of the form

$$\sum_{x=0}^{s} p_n(x) p_m(x) w(x) = d_n^2 \cdot \delta_{mn}, \quad 0 \leq m, n \leq s \qquad (5)$$

where d_n^2 denotes the square of the norm of the corresponding orthogonal polynomials and δ_{mn} denotes the Dirac function. Such polynomials include Tchebichef, Krawtchouk, Hahn, Meixner and Charlier polynomials. The normalised orthogonal polynomials can be obtained by utilising the square norm and weighted function

$$\tilde{p}_n(x) = p_n(x)\sqrt{\frac{w(x)}{d_n^2}}, \quad n = 0, 1, \ldots, s \quad (6)$$

Therefore the orthogonal property of normalised orthogonal polynomials in (5) can be rewritten as

$$\sum_{x=0}^{s} \tilde{p}_m(x)\tilde{p}_n(x) = \delta_{mn}, \quad 0 \le m, n \le s \quad (7)$$

For classical discrete orthogonal polynomials, Nikiforov and Uvarov [11] introduced some basis information listed in Table 1. Their weight functions are defined in the following discrete domain

$$G = \{x | 0 \le x \le s\} \quad (8)$$

Here, s is $N-1$ for discrete Tchebichef, Hahn polynomials and N for Krawtchouk polynomials. An unlimited discrete domain is holding for Meixner and Charlier polynomials.

A general form for obtaining the normalised discrete orthogonal polynomials $\tilde{p}_n(x)$ can be written as follows

$$A\tilde{p}_n(x) = B \cdot D\tilde{p}_{n-1}(x) + C \cdot E\tilde{p}_{n-2}(x) \quad (9)$$

where coefficients $A{-}E$ can be calculated according to (2), (3), (6) and Table 1. Equation (9) is a recurrence relation with respect to the polynomial order n.

3 Computation of discrete orthogonal polynomials

3.1 Recurrence relation with respect to n

In this subsection, we attempt to enumerate several classical discrete orthogonal polynomials by using the proposed general form (9).

3.1.1 Tchebichef polynomials: According to (1) and Table 1, one can obtain the first-order linear partial difference equation of Tchebichef orthogonal polynomials $t_n(x; N)$ as follows

$$x(N-x)\Delta\nabla t_n(x; N) + (N-1-2x)\Delta t_n(x; N) + n(n+1)t_n(x; N) = 0 \quad (10)$$

Tchebichef polynomials of order n, $n = 0, 1, \ldots, N-1$, are

Table 1 Data for Tchebichef $t_n(x; N)$, Krawtchouk $k_n(x; p, N)$, Hahn $h_n^{(a,b)}(x; N)$, Meixner $\varpi_n^{(\beta,\mu)}(x)$ and Charlier $c_n^{a_1}(x)$ polynomials, ($0 < p < 1$ for Krawtchouk, $a > 0$, $b > 0$ for Hahn, $\beta > 0$, $0 < \mu < 1$ for Meixner and $a_1 > 0$ for Charlier)

$p_n(x)$	$t_n(x; N)$	$k_n(x; p, N)$	$h_n^{(a,b)}(x; N)$	$\varpi_n^{(\beta,\mu)}(x)$	$c_n^{a_1}(x)$
s	$N-1$	N	$N-1$	∞	∞
$\sigma(x)$	$x(N-x)$	x	$x(N+a-x)$	x	x
$\tau(x)$	$N-1-2x$	$\dfrac{Np-x}{1-p}$	$(b+1)(N-1)-(a+b+2)x$	$\beta\mu - x(1-\mu)$	$a_1 - x$
λ_n	$n(n+1)$	$\dfrac{n}{1-p}$	$n(a+b+n+1)$	$n(1-\mu)$	n
B_n	$\dfrac{(-1)^n}{n!}$	$\dfrac{(-1)^n(1-p)^n}{n!}$	$\dfrac{(-1)^n}{n!}$	$\dfrac{1}{\mu^n}$	$\dfrac{1}{a_1^n}$
$w_n(x)$	$\dfrac{\Gamma(N-x)\Gamma(n+1+x)}{\Gamma(N-n-x)\Gamma(x+1)}$	$\dfrac{N!p^{x+n}(1-p)^{N-n-x}}{\Gamma(x+1)\Gamma(N+1-n-x)}$	$\dfrac{\Gamma(N+a-x)\Gamma(n+b+1+x)}{\Gamma(N-n-x)\Gamma(x+1)}$	$\dfrac{\mu^{x+n}\Gamma(n+\beta+x)}{\Gamma(\beta)x!}$	$\dfrac{e^{-a_1}a_1^{x+n}}{x!}$
d_n^2	$\dfrac{(N+n)!}{(2n+1)(N-n-1)!}$	$\dfrac{N!}{n!(N-n)!}(p(1-p))^n$	$\dfrac{\Gamma(a+n+1)\Gamma(b+n+1)(a+b+n+1)_N}{(a+b+2n+1)n!(N-n-1)!}$	$\dfrac{n!(\beta)_n}{\mu^n(1-\mu)^\beta}$	$\dfrac{n!}{a_1^n}$
α_n	$\dfrac{n+1}{2(2n+1)}$	$n+1$	$\dfrac{(n+1)(a+b+n+1)}{(a+b+2n+1)(a+b+2n+2)}$	$\dfrac{\mu}{\mu-1}$	$-a_1$
β_n	$\dfrac{N-1}{2}$	$n+p(N-2n)$	$\dfrac{a-b+2N-2}{4}$ $+\dfrac{(b^2-a^2)(a+b+2N)}{4(a+b+2n)(a+b+2n+2)}$	$\dfrac{n+\mu(n+\beta)}{1-\mu}$	$n+a_1$
γ_n	$\dfrac{n(N^2-n^2)}{2(2n+1)}$	$p(1-p)(N-n+1)$	$\dfrac{(a+n)(b+n)(a+b+N+n)(N-n)}{(a+b+2n)(a+b+2n+1)}$	$\dfrac{n(n-1+\beta)}{\mu-1}$	$-n$

also defined by using hypergeometric function as follows

$$t_n(x; N) = (1 - N)_{n3} F_2(-n, -x, 1 + n; 1, 1 - N; 1), \qquad (11)$$
$$n, x, y = 0, 1, 2, \ldots, N - 1$$

where $(a)_k = a(a + 1)(a + 2) \ldots (a + k - 1)$ is Pochhammer symbol. Using (2), (3), (6) and Table 1, the zero-order and first-order normalised Tchebichef polynomials can be calculated.

$$\tilde{t}_0(x; N) = \sqrt{1/N},$$
$$\tilde{t}_1(x; N) = (2x - N + 1)\sqrt{3/(N(N^2 - 1))} \qquad (12)$$

3.1.2 Krawtchouk polynomials:
Krawtchouk orthogonal polynomials with one variable $k_n(x; p, N)$ satisfy the following first-order partial difference equation

$$(1 - p)x\Delta\nabla k_n(x; p, N) + (Np - x)\Delta k_n(x; p, N)$$
$$+ nk_n(x; p, N) = 0, \quad 0 < p < 1 \qquad (13)$$

The nth Krawtchouk polynomial is defined by using hypergeometric function as

$$k_n(x; p, N) = {}_2F_1(-n, -x; -N; 1/p) \qquad (14)$$

The zero-order and first-order normalised Krawtchouk polynomials can be calculated using similar method used in calculating Tchebichef polynomials.

$$\tilde{k}_0(x; p, N) = \sqrt{\frac{N! p^x (1 - p)^{N-x}}{x!(N - x)!}}$$
$$\tilde{k}_1(x; p, N) = (-p(N - x) + x(1 - p)) \qquad (15)$$
$$\times \sqrt{\frac{(N - 1)! p^{x-1}(1 - p)^{N-x-1}}{x!(N - x)!}}$$

3.1.3 Hahn polynomials:
Hahn orthogonal polynomials with one variable $h_n^{(a,b)}(x; N)$ satisfy the following first-order partial differential equation of the form

$$x(N + a - x)\Delta\nabla h_n^{(a,b)}(x; N) + [(b + 1)(N - 1)$$
$$- (a + b + 2)x]\Delta h_n^{(a,b)}(x; N)$$
$$+ n(a + b + n + 1)h_n^{(a,b)}(x; N) = 0 \qquad (16)$$

where the parameters a and b are restricted to $a > 0$ and $b > 0$.

Hahn polynomials of order n, $n = 0, 1, \ldots, N - 1$ are also defined by using hypergeometric function as follows

$$h_n^{(a,b)}(x; N) = \frac{(-1)^n (b + 1)_n (N - n)_n}{n!}$$
$$\times {}_3F_2(-n, -x, n + 1 + a + b; b + 1, 1 - N; 1) \qquad (17)$$

A very important specific subclass of Hahn polynomials is

that when $a = b = 0$, it becomes Tchebichef system of the discrete polynomial $t_n(x; N)$. Similar to Tchebichef polynomials, the zero-order and first-order normalised Hahn can be calculated as follows

$$\tilde{h}_0^{(a,b)}(x; N) = \sqrt{\frac{w(x)}{d_0^2}}, \quad \tilde{h}_1^{(a,b)}(x; N) = ((a + b + 2)x$$
$$- (b + 1)(N - 1))\sqrt{\frac{w(x)}{d_1^2}} \qquad (18)$$

3.1.4 Meixner polynomials:
Meixner polynomials with one variable $\varpi_n^{(\beta,\mu)}(x)$ satisfy the following first-order partial differential equation of the form

$$x\Delta\nabla\varpi_n^{(\beta,u)}(x) + (\beta\mu - x(1 - \mu))\Delta\varpi_n^{(\beta,u)}(x)$$
$$+ n(1 - \mu)\varpi_n^{(\beta,u)}(x) = 0 \qquad (19)$$

where β and μ are restricted to $0 < \mu < 1$ and $\beta > 0$.

The nth Meixner polynomial is also defined by using hypergeometric function as follows

$$\varpi_n^{(\beta,u)}(x) = (\beta)_{n2} F_1(-n, -x; \beta; 1 - 1/\mu) \qquad (20)$$

Similarly, the zero-order and the first-order normalised Meixner can be calculated as follows

$$\tilde{\varpi}_0^{(\beta,\mu)}(x) = \sqrt{\frac{w(x)}{d_0^2}} = \sqrt{\frac{\mu^x(\beta + x - 1)!}{x!(\beta - 1)!}(1 - \mu)^\beta}$$
$$\tilde{\varpi}_1^{(\beta,\mu)}(x) = \left(\beta + x - \frac{x}{\mu}\right)\sqrt{\frac{w(x)}{d_1^2}} = \left(\beta + x - \frac{x}{\mu}\right) \qquad (21)$$
$$\times \sqrt{\frac{\mu^x(\beta + x - 1)!}{x!(\beta - 1)!}\frac{\mu(1 - \mu)^\beta}{\beta}}$$

3.1.5 Charlier polynomials:
Charlier polynomials with one variable $c_n^{a_1}(x)$ satisfy the following first-order partial differential equation of the form

$$x\Delta\nabla c_n^{a_1}(x) + (a_1 - x)\Delta c_n^{a_1}(x) + nc_n^{a_1}(x) = 0 \qquad (22)$$

where a_1 is restricted to $a_1 > 0$.

The nth Charlier polynomial is also defined by using hypergeometric function as follows

$$c_n^{a_1}(x) = {}_2F_0(-n, -x; \; ; -1/a_1) \qquad (23)$$

The zero-order and the first-order normalised Charlier can be

calculated as follows

$$\tilde{c}_0^{a_1}(x) = \sqrt{\frac{w(x)}{d_0^2}} = \sqrt{\frac{e^{-\mu}\mu^x}{x!}}$$

$$\tilde{c}_1^{a_1}(x) = \frac{\mu - x}{\mu}\sqrt{\frac{w(x)}{d_1^2}} = \frac{\mu - x}{\mu}\sqrt{\frac{e^{-\mu}\mu^{x+1}}{x!}}$$

(24)

The normalised discrete Tchebichef, Krawtchouk, Hahn, Meixner and Charlier polynomials satisfy the orthogonal condition (7), and the proposed general form (9), where

$\tilde{p}_n(x)$ is $\tilde{t}_n(x; N)$, $\tilde{k}_n(x; p, N)$, $\tilde{h}_n^{(a,b)}(x; N)$, $\tilde{\varpi}_n^{(\beta,\mu)}(x)$ or $\tilde{c}_n^{a_1}(x)$, respectively, for each polynomials listed in the order above. The coefficients $A–E$ in (9) are deduced and listed in Table 2, and the initial values are obtained through (12), (15), (18), (21) and (24), respectively.

3.2 Recurrence relation with respect to x

From the previous subsection, it is found that high-order polynomials can be deduced from the low-order polynomials. For example, polynomials ($\tilde{t}_n(x; N)$,

Table 2 Data for the three-term recurrence relation of Tchebichef, Krawtchouk, Hahn, Meixner and Charlier polynomials ($0 < p < 1$ for Krawtchouk, $a > 0$, $b > 0$ for Hahn, $\beta > 0$, $0 < \mu < 1$ for Meixner, and $a_1 > 0$ for Charlier polynomials)

$\tilde{p}_n(x)$	A	B	C
$\tilde{t}_n(x; N)$	$\dfrac{n}{2(2n-1)}$	$x - \dfrac{N-1}{2}$	$-\dfrac{(n-1)[N^2-(n-1)^2]}{2(2n-1)}$
$\tilde{k}_n(x; p, N)$	n	$x - n + 1 - p(N - 2n + 2)$	$-p(1-p)(N-n+2)$
$\tilde{h}_n^{(a,b)}(x; N)$	$\dfrac{n}{(a+b+2n-1)} \times \dfrac{(a+b+n)}{(a+b+2n)}$	$x - \dfrac{a-b+2N-2}{4} - \dfrac{(b^2-a^2)(a+b+2N)}{4(a+b+2n-2)(a+b+2n)}$	$-\dfrac{(a+n-1)(b+n-1)}{(a+b+2n-2)} \times \dfrac{(a+b+N+n-1)(N-n+1)}{(a+b+2n-1)}$
$\tilde{\varpi}_n^{(\beta,\mu)}(x)$	$\dfrac{\mu}{\mu - 1}$	$\dfrac{x - x\mu - n + 1 - \mu n + \mu - \beta\mu}{1-\mu}$	$\dfrac{(n-1)(n-2+\beta)}{1-\mu}$
$\tilde{c}_n^{a_1}(x)$	$-a_1$	$x - n + 1 - a_1$	$n - 1$

D	E
$\sqrt{\dfrac{(2n+1)}{(N^2-n^2)(2n-1)}}$	$\sqrt{\dfrac{2n+1}{(N^2-n^2)[N^2-(n-1)^2](2n-3)}}$
$\sqrt{\dfrac{n}{p(1-p)(N-n+1)}}$	$\sqrt{\dfrac{n(n-1)}{(p(1-p))^2(N-n+2)(N-n+1)}}$
$\sqrt{\dfrac{n(a+b+n)(a+b+2n+1)}{(N-n)(a+n)(b+n)(a+b+2n-1)(a+b+n+N)}}$	$\sqrt{\dfrac{n(n-1)(a+b+n)}{(a+n)(a+n-1)(b+n)(b+n-1)(N-n+1)(N-n)}} \times \sqrt{\dfrac{(a+b+n-1)(a+b+2n+1)}{(a+b+2n-3)(a+b+n+N)(a+b+n+N-1)}}$
$\sqrt{\dfrac{u}{n(\beta+n-1)}}$	$\sqrt{\dfrac{u^2}{n(n-1)(\beta+n-2)(\beta+n-1)}}$
$\sqrt{\dfrac{a_1}{n}}$	$\sqrt{\dfrac{a_1^2}{n(n-1)}}$

$\tilde{k}_n(x; p, N)$, $\tilde{h}_n^{(a,b)}(x; N))$ are the polynomials at x^n, thus, the term ($\tilde{t}_{N-1}(N-1; N)$, $\tilde{k}_{N-1}(N-1; p, N)$, $\tilde{h}_{N-1}^{(a,b)}(N-1; N)$) at $N = 100$ must contain the term 100^{100} multiplied by an infinitely small coefficient so that the magnitude is less than 1. Thus, the computation of the discrete moments in larger orders causes the propagation of numerical errors while using the recurrence relation for evaluating the polynomials' values. Consequently, the numerical instability will severely affect the quality of image reconstruction, particularly for large image (larger than 100×100 pixels). To remedy this problem, Mukundan proposed a solution to compute Tchebichef polynomials by modifying the recurrence relation [16]. The x recurrence relation is used instead of n recurrence relation to avoid errors accumulating in the result. This subsection will introduce another general form of their recurrence relations with respect to x.

Considering the properties of the operator ∇ and Δ, we have

$$\Delta \nabla p_n(x) = p_n(x+1) - 2p_n(x) + p_n(x-1) \qquad (25)$$

Thus, the recurrence relations of discrete orthogonal polynomials with respect to x can be obtained through (1) and (25) as follows

$$p_n(x) = \frac{2\sigma(x-1) + \tau(x-1) - \lambda_n}{\sigma(x-1) + \tau(x-1)} p_n(x-1)$$
$$- \frac{\sigma(x-1)}{\sigma(x-1) + \tau(x-1)} p_n(x-2) \qquad (26)$$

According to (6) and (26), another general form for obtaining discrete orthogonal polynomials is written as follows. It is a recurrence relation with respect to x.

$$\tilde{p}_n(x) = \frac{\sqrt{w(x)}}{\sigma(x-1) + \tau(x-1)} \left[\frac{2\sigma(x-1) + \tau(x-1) - \lambda_n}{\sqrt{w(x-1)}} \right.$$
$$\left. \times \tilde{p}_n(x-1) - \frac{\sigma(x-1)}{\sqrt{w(x-2)}} \tilde{p}_n(x-2) \right]$$
$$(27)$$

Thus, one can obtain the recurrence relations of discrete Tchebichef, Krawtchouk, Hahn, Meixner and Charlier polynomials with respect to x according to the general form (27) and Table 1, where $\tilde{p}_n(x)$ is $\tilde{t}_n(x; N)$, $\tilde{k}_n(x; p, N)$, $\tilde{h}_n^{(a,b)}(x; N)$, $\tilde{\varpi}_n^{(\beta,\mu)}(x)$ or $\tilde{c}_n^{a_1}(x)$, respectively.

Using (2), (3), (6) and Table 1, we obtain the initial values of recurrence relation with respect to x listed in Table 3. The above equations can be used to calculate the weighted Tchebichef, Krawtchouk, Hahn, Meixner and Charlier polynomials' values effectively. Fig. 1 shows the plots of the first few orders of these polynomials with different parameter values. Fig. 1a shows that Tchebichef polynomials' ROI spreads all along x-axis. Figs. 1b−d show that Krawtchouk polynomials' ROI is shifted horizontally when using different parameter p; if $p < 0.5$, ROI is shifted to the left of the central x value as shown in Fig. 1c; while for $p > 0.5$, ROI is shifted to the right of it as shown in Fig. 1d. For Hahn polynomials, parameters a and b are together responsible for shifting the ROI. The smaller the value of b, the further left the ROI will be, as shown in Fig. 1f. Similarly, the ROI shifts to the further right when b is larger shown in Fig. 1g. This property is useful for

Table 3 Initial values of the three-term recurrence relation with respect to x for Tchebichef, Krawtchouk, Hahn, Meixner and Charlier polynomials ($a > 0$, $b > 0$ for Hahn, $0 < p < 1$ for Krawtchouk, $0 < \mu < 1$, $\beta > 0$ for Meixner, $a_1 > 0$ for Charlier polynomials)

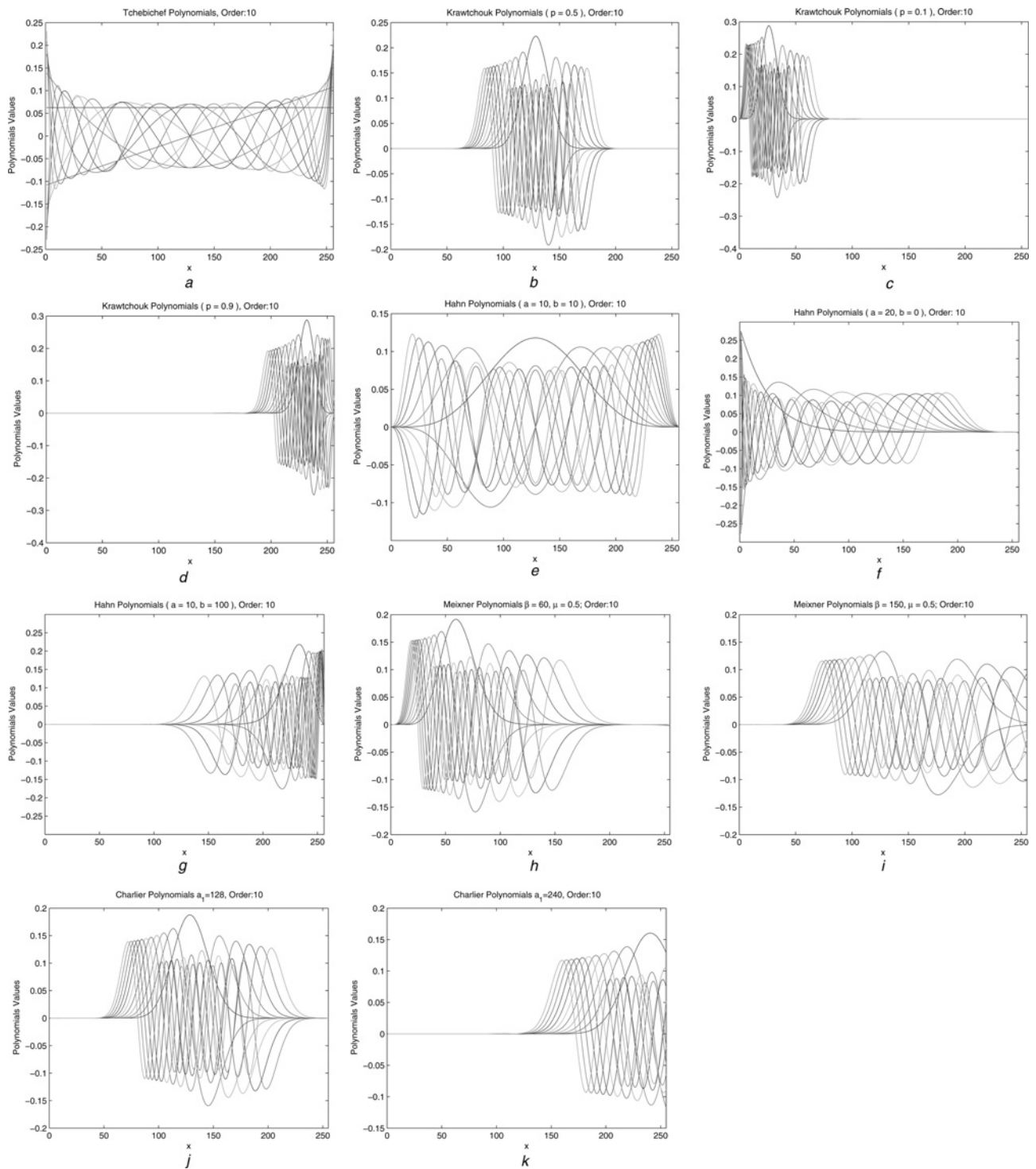| $\tilde{p}_n(x)$	$x = 0$	$x = 1$
$\tilde{t}_n(x; N)$	$(-1)^n (N-n)_n \sqrt{\dfrac{w(0)}{d_n^2}}$	$\left(1 + \dfrac{n(n+1)}{1-N}\right) \sqrt{\dfrac{w(1)}{w(0)}} \tilde{t}_n(0; N)$
$\tilde{k}_n(x; p, N)$	$(-1)^n \dbinom{N}{n} p^n \sqrt{\dfrac{w(0)}{d_n^2}}$	$\dfrac{(N-n)p - n(1-p)}{Np} \sqrt{\dfrac{w(1)}{w(0)}} \tilde{k}_n(0; p, N)$
$\tilde{h}_n^{(a,b)}(x; N)$	$(1-N)_n \dbinom{n+b}{n} \sqrt{\dfrac{w(0)}{d_n^2}}$	$\dfrac{(n+b+1)(N-n-1) - n(N+a-1)}{(b+1)(N-1)} \sqrt{\dfrac{w(1)}{w(0)}} \tilde{h}_n^{(a,b)}(0; N)$
$\tilde{\varpi}_n^{(\beta,\mu)}(x)$	$(\beta)_n \sqrt{\dfrac{w(0)}{d_n^2}}$	$\dfrac{\mu(n+\beta) - n}{\mu\beta} \sqrt{\dfrac{w(1)}{w(0)}} \tilde{\varpi}_n^{(\beta,\mu)}(0)$
$\tilde{c}_n^{a_1}(x)$	$\sqrt{\dfrac{w(0)}{d_n^2}}$	$\dfrac{a_1 - n}{a_1} \sqrt{\dfrac{w(1)}{w(0)}} \tilde{c}_n^{a_1}(0)$

Figure 1 *Plots of normalised polynomials when N = 256, order's number = 10*

a Tchebichef
b Krawtchouk ($p = 0.5$)
c Krawtchouk ($p = 0.1$)
d Krawtchouk ($p = 0.9$)
e Hahn ($a = 10$, $b = 10$)
f Hahn ($a = 20$, $b = 0$)
g Hahn ($a = 10$, $b = 100$)
h Meixner ($\beta = 60$, $\mu = 0.5$)
i Meixner ($\beta = 150$, $\mu = 0.5$)
j Charlier ($a_1 = 128$)
k Charlier ($a_1 = 240$)

image description and pattern recognition. For the Meixner and Charlier polynomials, this phenomenon is not obvious as shown in Figs. 1*h*−1*k*. Fig. 1 illustrates that polynomial's parameters play an important role in pattern recognition task. Discussions of these parameters applied in pattern recognition are beyond this study. We shall detail them in another literature.

4 Discrete orthogonal moments

In this section, s is $N-1$ for Tchebichef and Hahn polynomials, s is N for Krawtchouk polynomials and $s \geq 0$ for Meixner and Charlier polynomials.

4.1 One-dimensional discrete orthogonal moments

The discrete orthogonal moments are a set of moments formed by the normalised polynomials. The one-dimensional discrete orthogonal moment set is defined as

$$v_n = \sum_{x=0}^{N-1} \tilde{p}_n(x) f(x), \quad n = 0, 1, \ldots, s \qquad (28)$$

where $f(x)$ is one-dimensional signal with length N. If the set of moment's v_n is given from order 0 up to M, the moment-based signal reconstruction is as follows

$$\hat{f}(x) \simeq \sum_{n=0}^{M} v_n \tilde{p}_n(x), \quad x = 0, 1, \ldots, N-1 \qquad (29)$$

Here, one refers the normalised discrete orthogonal polynomials $\tilde{p}_n(x)$ to the general form (9) or (27).

4.2 Two-dimensional discrete orthogonal moments

One of the most frequent applications of the moment functions is image processing and pattern recognition so that it must be extensible to two-dimensions. The discrete orthogonal moments presented in this paper have the separable basis functions. Owing to the separability that the basis function has, the moments can be computed in two steps: 1-D operations on the rows of an image and 1-D operations on the columns. Fig. 2 shows the basis functions of several discrete orthogonal moments for a block size 8×8. It is noted that the basis functions exhibit a progressive increase in frequency in both vertical and horizontal direction. The top is referred as DC coefficient and holds a constant value.

Given a digital image $f(x, y)$ with size $N \times N$, that is, $x \in [0, \ N-1]$ and $y \in [0, \ N-1]$, the $(l+m)$th-order moments with a variable orthogonal polynomials as basis function for an image is defined as follows

$$M_{lm} = \sum_{x=0}^{N-1} \sum_{y=0}^{N-1} f(x, y) \tilde{p}_l(x) \tilde{p}_m(y), \qquad (30)$$

$$l, m = 0, 1, \ldots, s$$

We can simply use the following matrix notation

$$\boldsymbol{M} = \boldsymbol{P}_x^{\mathrm{T}} \boldsymbol{f} \boldsymbol{P}_y \qquad (31)$$

where $\boldsymbol{f}$ denotes $N \times N$ image matrix and

$$\boldsymbol{P}_x = [\tilde{p}_0(x), \tilde{p}_1(x), \ldots, \tilde{p}_s(x)]^{\mathrm{T}},$$
$$\boldsymbol{P}_y = [\tilde{p}_0(y), \tilde{p}_1(y), \ldots, \tilde{p}_s(y)]^{\mathrm{T}} \qquad (32)$$

and

$$\tilde{p}_n(x) = [\tilde{p}_n(0), \tilde{p}_n(1), \ldots, \tilde{p}_n(N-1)]^{\mathrm{T}},$$
$$n = 0, 1, \ldots, s \qquad (33)$$

Using (30) also leads to the following inverse moment transform

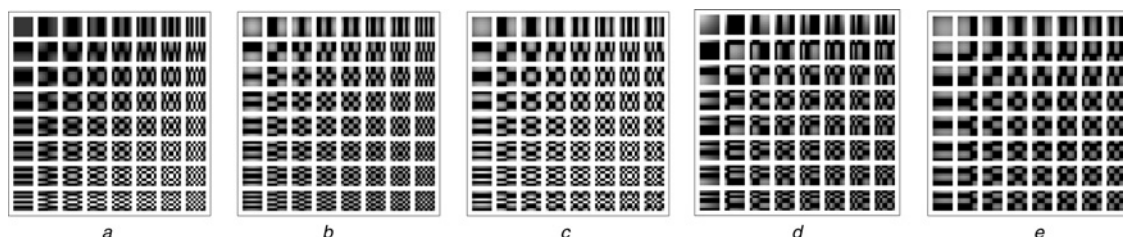$$f(x, y) = \sum_{l=0}^{s} \sum_{m=0}^{s} M_{lm} \tilde{p}_l(x) \tilde{p}_m(y) \qquad (34)$$

Figure 2 *Basis functions of several discrete orthogonal moments (N = 8)*

a TM
b KM ($p_1 = p_2 = 0.5$)
c HM ($a_1 = b_1 = a_2 = b_2 = 10$)
d MM ($\beta_1 = \beta_2 = 4$, $\mu_1 = \mu_2 = 0.2$)
e CM ($a_1 = a_2 = 5$)
Neutral white colour represents one, white colour represents positive amplitudes and black colour represents negative amplitudes

Similarly, the inverse reconstruction procedure can be represented using the matrix as

$$f = P_x M P_y^T \qquad (35)$$

If moments are limited to an order K, we can approximate f by $\hat{f}$.

$$\hat{f}(x, y) = \sum_{l=0}^{K} \sum_{m=0}^{l} M_{l-m,m} \tilde{p}_{l-m}(x) \tilde{p}_m(y),$$
$$x, y = 0, 1, \ldots, N-1 \qquad (36)$$

Matrix representation methods are used to describe the reconstruction process as

$$\tilde{P}_x = [\tilde{p}_0(x), \tilde{p}_1(x), \ldots, \tilde{p}_K(x)]^T,$$
$$\tilde{P}_y = [\tilde{p}_0(y), \tilde{p}_1(y), \ldots, \tilde{p}_K(y)]^T \qquad (37)$$

and then yield the moment matrix $\tilde{M}$ using (31) and (37). The approximation of an image can be solved in an analogous way, as shown in (35).

5 Properties of discrete orthogonal moments

The discussions in the preceding sections have developed a mathematical foundation for several discrete orthogonal moments. However, the intuitive insight into its image processing application by using proposed two general forms has not been presented. This section outlines (with examples) some properties of several orthogonal moments which are of particular value to image processing application. Fig. 3 shows several sample images. Among them, Hill and Lena with size 256×256 were frequently used in image processing and chosen here for the analysis of the properties of the proposed moment functions. Other test images' sizes are 256×256, including 'Sea' and 'Ducks'. Besides the image Ducks, the grey-levels are represented using 8-bit.

The procedure for calculating moments' values is the procedure of orthogonal transformation. In this study, we use term 'moments' for consistency. Many different transforms have been considered for speech and image coding, such as discrete cosine transformation (DCT) and Karhunen–Loève transform (KLT). These methods differ in their abilities of performing energy compaction and signal decorrelation. The main objective of Sections 5.1 and 5.2 is to compare the performance of one-dimensional Tchebichef, Krawtchouk and Hahn moments using two criteria, such as energy compaction and decorrelation capability. A standard way of comparing the transforms is based on the assumption that the signal x satisfies the first-order Markov model with a correlation coefficient ρ [17]. This model has been used extensively in digital image coding [18]. For example, this method was adopted for comparing DCT and KLT [17, 19]. Thus, the following comparisons in terms of energy compaction and decorrelation are all based on this particular model. Here, we only consider the polynomials whose weight functions are defined in a finite discrete domain. It is because that the evaluation method used here is effective in such a domain.

5.1 Energy compaction

Consider a first-order zero mean stationary Markov sequence with length N whose covariance matrix R is given by (38) with different covariance coefficient ρ.

$$\mathbf{R} = \begin{bmatrix} 1 & \rho & \rho^2 & \cdots & \rho^{N-1} \\ \rho & \ddots & \ddots & \ddots & \vdots \\ \vdots & \ddots & \ddots & \ddots & \rho^2 \\ \vdots & & \ddots & \ddots & \rho \\ \rho^{N-1} & & & \rho & 1 \end{bmatrix} \qquad (38)$$

Table 4 lists variance σ_k^2 of the transform coefficients (in decreasing order) for Tchebichef, Krawtchouk and Hahn moments. To compare the energy compaction capability, the normalised basis restriction error J_m defined by Jain [17] is used here.

$$J_m = \frac{\sum_{k=m}^{N-1} \sigma_k^2}{\sum_{k=0}^{N-1} \sigma_k^2}, \qquad m = 0, \ldots, N-1 \qquad (39)$$

Figure 3 *Test images (size: 256 × 256)*

a Hill
b Lena
c Sea
d Ducks

Table 4 Variances σ_k^2 of several transform coefficients of a stationary Markov sequence in different correlation coefficient ρ

	$\rho = 0.95, N = 16$			$\rho = 0.85, N = 16$		
k	Tchebichef	Krawtchouk	Hahn	Tchebichef	Krawtchouk	Hahn
0	12.41	8.220	9.786	7.962	6.230	7.056
1	1.901	1.115	1.486	3.250	2.275	2.843
2	0.6111	2.916	2.459	1.530	2.277	2.140
3	0.3001	0.714	0.615	0.853	1.349	1.198
4	0.182	1.413	0.807	0.543	1.193	0.839
5	0.1242	0.393	0.227	0.380	0.746	0.489
6	0.0922	0.599	0.233	0.285	0.579	0.332
7	0.0722	0.169	0.083	0.224	0.352	0.217
8	0.059	0.192	0.071	0.184	0.249	0.165
9	0.049	0.064	0.044	0.155	0.164	0.134
10	0.043	0.057	0.039	0.135	0.127	0.118
11	0.038	0.034	0.034	0.119	0.105	0.107
12	0.034	0.031	0.031	0.107	0.096	0.099
13	0.031	0.028	0.029	0.098	0.089	0.092
14	0.029	0.027	0.028	0.090	0.086	0.087
15	0.027	0.026	0.026	0.084	0.083	0.083

where σ_k^2 has been arranged in the decreasing order. Fig. 4 shows J_m against m for various moments while covariance coefficient ρ is from 0.8 to 0.95. It is seen that the performance of Tchebichef moments is distinguishable from those of other moments. Hahn moment is the suboptimal transform among them.

5.2 Signal decorrelation

The principal advantage of the orthogonal transformation is the removal of redundancy between neighbouring pixels. This led to the fact that uncorrelated transform coefficients are able to be encoded independently. To quantitatively compare the signal decorrelation of an orthogonal transform, a residual correlation (RC) measure was defined by Hamidi and Peral [19] as

$$ \text{RC} = \frac{||\boldsymbol{R} - \boldsymbol{R}_U||^2}{||\boldsymbol{R} - \boldsymbol{I}||^2} \qquad (40) $$

where $|| \ ||^2$ denotes the Hilbert−Schmide weak norm which is defined as the sum of squares of a matrix divided by its dimension N. $\boldsymbol{I}$ is the identity matrix. $\boldsymbol{R}$ is a Toeplitz matrix of the form deduced from (38) and U is an orthogonal transform. Let $\boldsymbol{R}' = U\boldsymbol{R}U^{-1}$ be the representation of $\boldsymbol{R}$ in the new basis, and $\boldsymbol{R}'_U = \text{diag}(R'_{11}, R'_{22}, \ldots, R_{MM})$. We define $\boldsymbol{R}_U$ the representation of $\boldsymbol{R}'_U$ in

the first basis, that is

$$ \boldsymbol{R}_U = U^{-1}\boldsymbol{R}'_U U \qquad (41) $$

and $||\boldsymbol{R} - \boldsymbol{R}_U||^2$ is the Hilbert−Schmidt norm of $\boldsymbol{R} - \boldsymbol{R}_U$, that is

$$ ||\boldsymbol{R} - \boldsymbol{R}_U||^2 = \frac{1}{M}\left(\sum_{m,n=0}^{M-1}|(\boldsymbol{R} - \boldsymbol{R}_U)_{mn}|^2\right) \qquad (42) $$

The comparison here is based on the first-order Markov model for the input sequence. Fig. 5 shows the RC plot for $M = 8$. Hahn moments perform better than Krawtchouk moments in a wide region of ρ, that is, $0.01 < \rho < 1$. With the increasing of correlations, the advantage of Tchebichef moments over the others becomes more significant. For many images, ρ is found to be around 0.95 [17, p. 37], and Tchebichef moments perform better than Krawtchouk and Hahn moments in this region.

5.3 Experiments about energy compaction in real images

Compressing image in the spatial domain is difficult because image's energy often varies significantly throughout the whole image; however, images tend to have a compact representation in the frequency domain packed around low
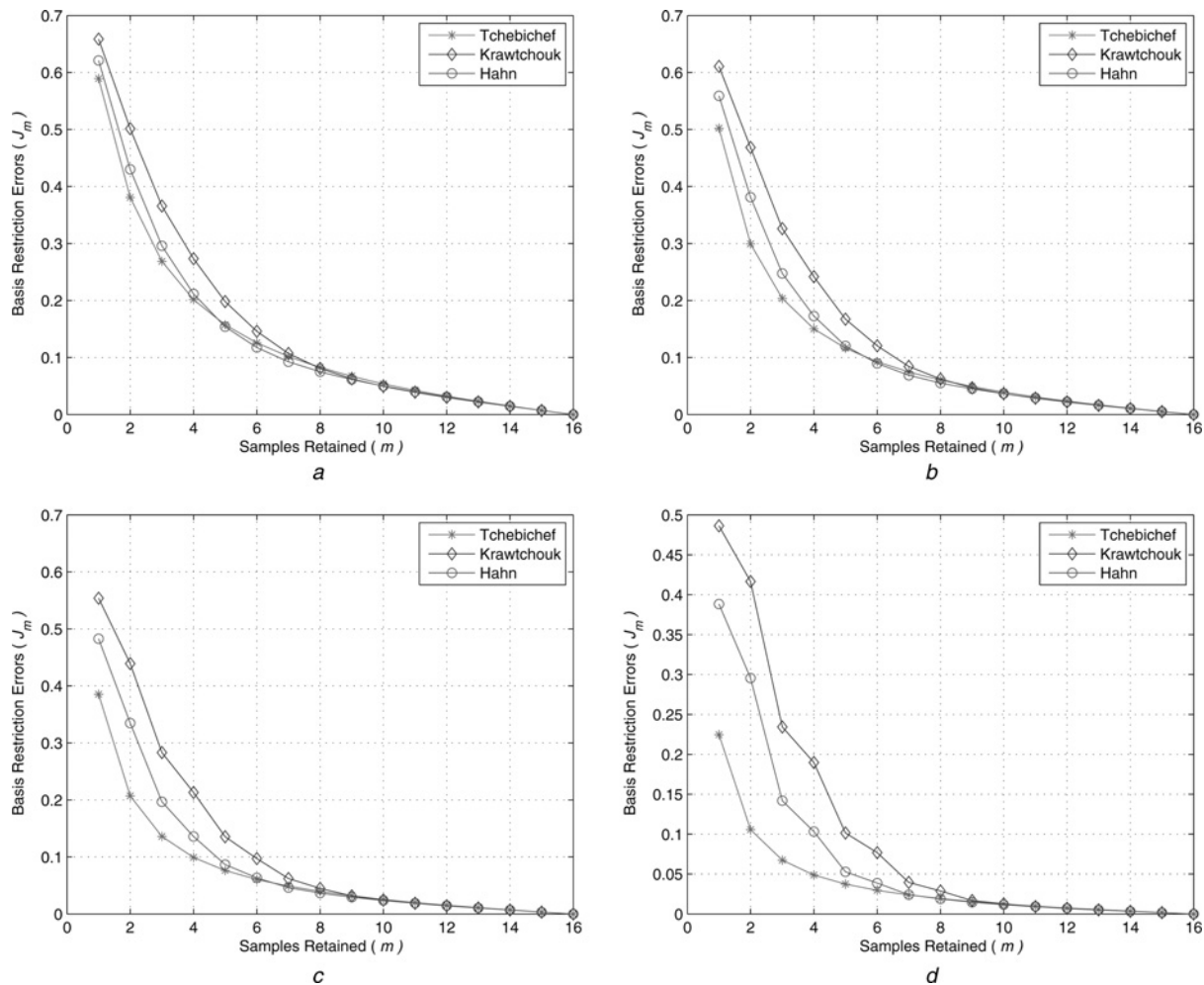
Figure 4 *Performance of different unitary transforms by showing basis restriction errors (J_m) against the number of basis (m) for a stationary Markov sequence with N = 16, p = 0.5 for Krawtchouk, and a = b = 10 for Hahn moments*

a $\rho = 0.8$
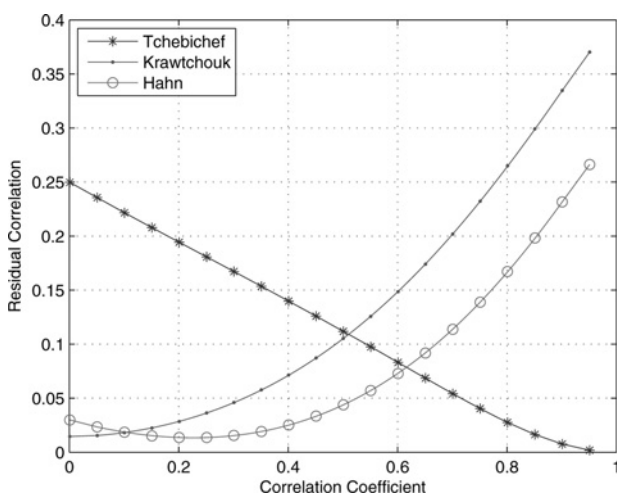b $\rho = 0.85$
c $\rho = 0.9$
d $\rho = 0.95$

Figure 5 *Comparison of the RCs among the several orthogonal moments for a first-order Markov sequence when N = 8 and 0 < ρ < 1, p = 0.5 for Krawtchouk, and a = b = 10 for Hahn moments*

frequencies which make the compression in a frequency domain more efficient. Moments based on discrete orthogonal polynomials are usually used in image compression. It is because they exhibit a better energy compaction for common images. If a discrete orthogonal moment is properly chosen, the energy in an image will be concentrated on a relatively small percentage of the moment coefficients; these coefficients are quantised, stored and then later used for generating the reconstructed image. Saving few coefficients yields an extremely high compression ratio but a rather noisy reconstructed image, whereas more coefficients give a clear image but lower compression efficiency.

The purpose of this experiment is to confirm and compare the energy compact of several proposed moment functions. The compression experiments were conducted on three test images. According to the compression ratio, the absolute value of all transform coefficients are rearranged in downward order, and part of them are chosen to reconstruct

Figure 6 *Decoded images using various discrete orthogonal moments, compression ratio 4:1, block size 16*

a TM
b KM ($p_1 = p_2 = 0.5$)
c HM ($a_1 = b_1 = a_2 = b_2 = 10$)

the original image according to the compression ratio. Fig. 6 shows the decoded results of the test image Lena. In this experiment, the compression ratio is set to 4:1 and the block size is set to 16×16. The parameter concerned in Krawtchouk polynomials is chosen as $p_1 = p_2 = 0.5$ and $a_1 = b_1 = a_2 = b_2 = 10$ for Hahn polynomials.

In order to evaluate the performance of different methods, we use peak signal-to-noise ratio (PSNR) to quantitatively measure the fidelity of the decoded image. The PSNR of a grey-level image is defined as

$$\mathrm{PSNR} = 10 \log_{10} \left(\frac{255^2}{\mathrm{mse}} \right) \qquad (43)$$

where 255 is the peak image amplitude, mse is the mean square error (MSE) which is defined as follows

$$\mathrm{mse} = \frac{1}{N^2} \sum_{x=0}^{N-1} \sum_{y=0}^{N-1} [f(x, y) - \hat{f}(x, y)]^2 \qquad (44)$$

where $f(x, y)$ and $\hat{f}(x, y)$ denote the original image and the reconstructed image, respectively. Table 5 lists the PSNR of different methods for three test images with compression ratio 4:1 and 8:1, respectively. It can be clearly seen from Table 5 that the JPEG 2000 provides the highest PSNR throughout all the tests. The moments constructed by Tchebichef have better compression behaviour than those

of Krawtchouk and Hahn polynomials. This conclusion is consistent with the theoretical analysis in the previous subsection.

5.4 Global feature extraction

In this subsection, the global feature extraction capability of the proposed moments is verified by reconstructing the complete images. Two test images, Hill and Sea, are used to illustrate the effectiveness of these moments. We first investigate the discrete orthogonal moments whose corresponding weight function is restricted in a limited domain, such as Tchebichef, Krawtchouk and Hahn moments. Owing to the influence of parameters p on Krawtchouk polynomials, and parameters a, b on Hahn polynomials, the region of emphasis of the proposed moments can be controlled. This is indicated in Fig. 1. Therefore the proposed moments can be set into global or local feature extraction mode by setting parameters p, a and b. While the parameters $p_1 = p_2 = 0.5$ for Krawtchouk polynomials and $a_1 = b_1 = a_2 = b_2$ for Hahn polynomials, the Krawtchouk moments and Hahn moments are set into global feature extraction mode.

Fig. 7 shows the reconstruction results of image Hill using different moments with a maximum order of up to 255. To measure the accuracy of the reconstructed image, we use the mse defined by (44) to measure the performance of the reconstruction. Fig. 8 shows the detailed plots of the corresponding mse using three different orthogonal moments with a maximum order of up to 255. Note that the reconstruction errors decrease monotonically with the increase of the number of orders as predicted. We observe that the reconstruction results based on KM are better than those based on TM and HM. Fig. 8 illustrates that HM is not as good as KM. However, it outperforms TM. In this experiment, the parameters of moments are set to global feature extraction mode, that is, $p_1 = p_2 = 0.5$ for Krawtchouk and $a_1 = b_1 = a_2 = b_2 = 10$ for Hahn polynomials. We draw the conclusion that the KM has better global feature extraction than other moments. The moments whose polynomials are constructed by Tchebichef have weak global extraction capability.

Table 5 Lists of peak signal-to-noise ratio values (PSNR in dB) to indicate the compression efficiency

Images	Hill		Lena		Sea	
compression ratio	4:1	8:1	4:1	8:1	4:1	8:1
TM	32.64	29.35	34.25	30.29	32.15	28.34
KM	30.50	25.24	31.57	24.80	30.50	24.05
HM	31.89	27.63	33.81	28.14	32.06	26.84
JPEG	33.13	30.30	47.31	38.28	36.51	30.26
JPEG 2000	35.26	31.04	48.25	39.13	37.52	32.31

Reconstructed images using TM

Reconstructed images using KM ($p_1 = p_2 = 0.5$)

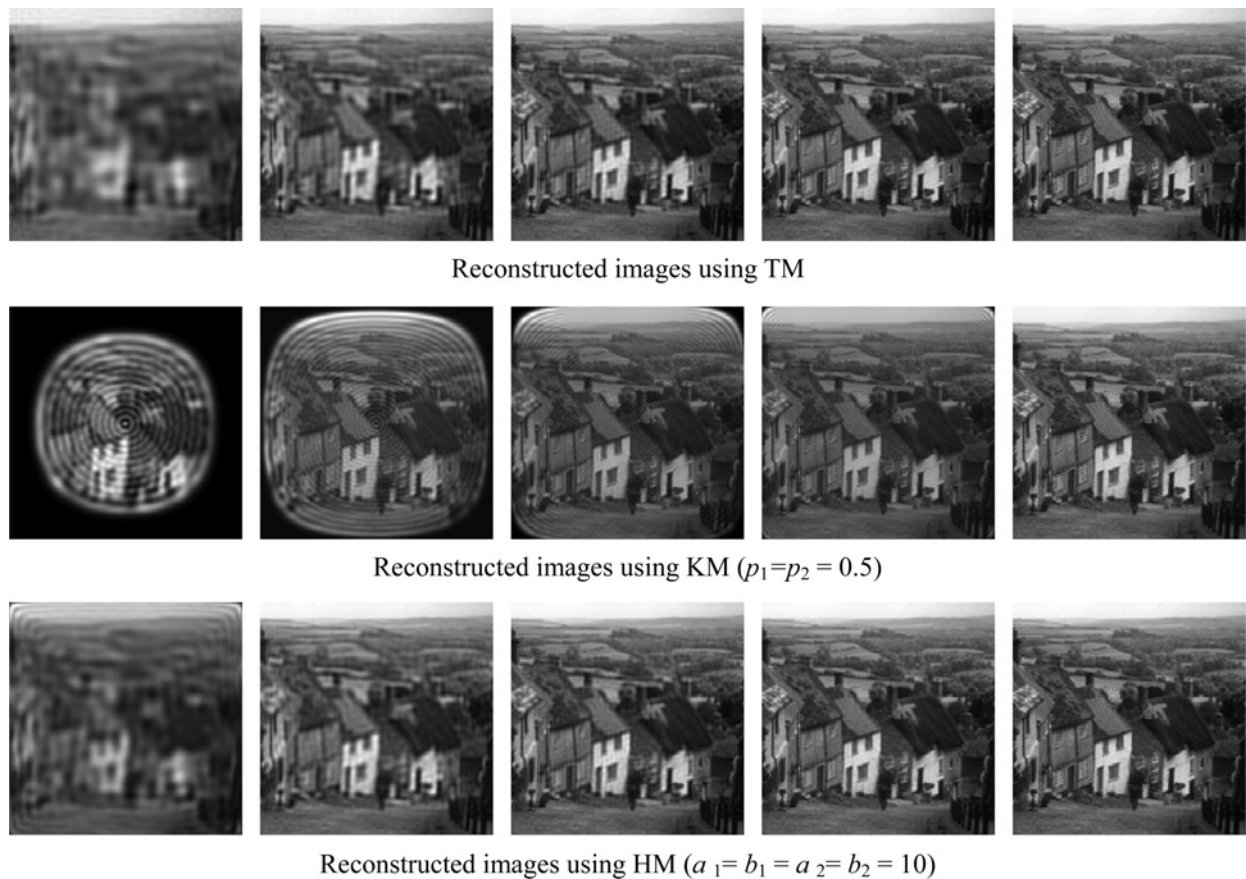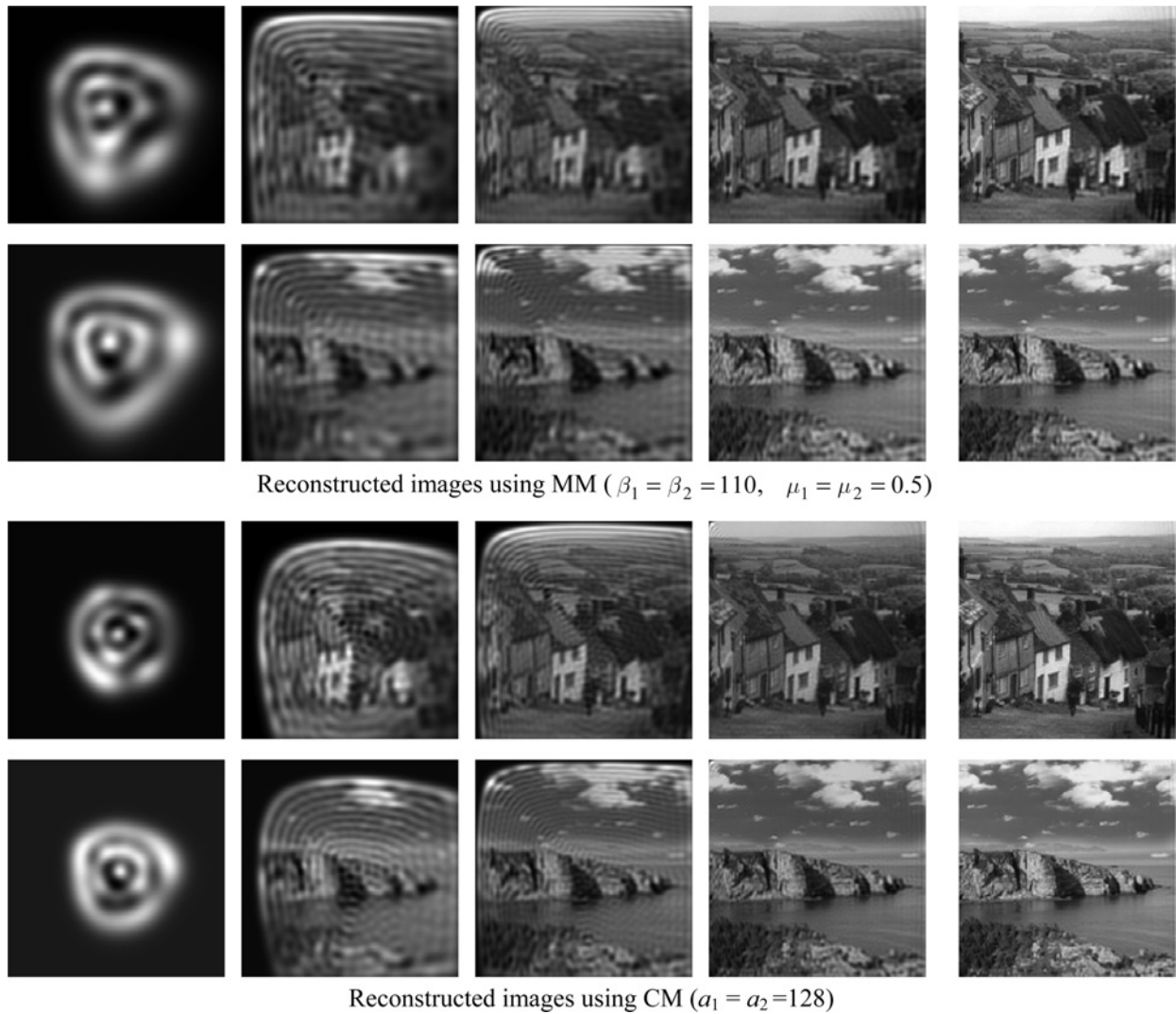Reconstructed images using HM ($a_1 = b_1 = a_2 = b_2 = 10$)

Figure 7 *Reconstruction of the grey-level image Hill*

The order's numbers from left to right are 50, 100, 150, 200 and 255, respectively

In the following experiments, test images, Hill and Sea, are still used to compare the performance by using the proposed methods MM and CM. In these moment functions, the polynomials Meixner and Charlier, which are orthogonal in an unlimited interval $[0, \infty]$, are used as basis functions of moments. Both reconstructed images and a detailed comparison of the variation of reconstruction errors are shown in Figs. 9 and 10, respectively. Comparing Figs. 8 and 10, it is found that the global description capability of MM and CM is lower than those of TM, KM and HM, while the same order of the moments is calculated. Owing to the fact that Meixner and Charlier polynomials are
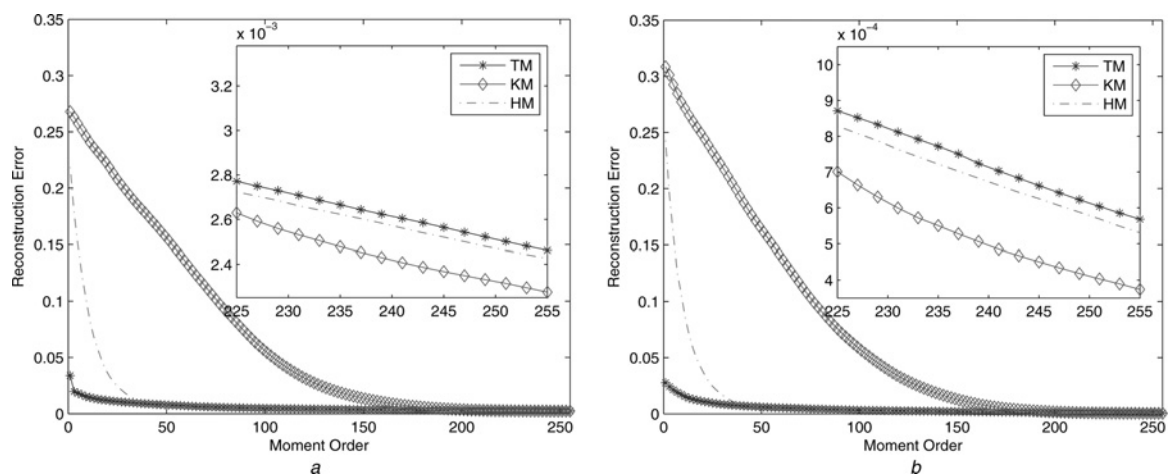
Figure 8 *Comparative study of reconstruction errors by using TM, KM ($p_1 = p_2 = 0.5$) and HM ($a_1 = b_1 = a_2 = b_2 = 10$) in two different images*

a Errors from test image Hill
b Errors from test image Sea

Reconstructed images using MM ($\beta_1 = \beta_2 = 110, \quad \mu_1 = \mu_2 = 0.5$)

Reconstructed images using CM ($a_1 = a_2 = 128$)

Figure 9 *Reconstruction of the grey-level images Hill and Sea*

The order's numbers from left to right are 10, 50, 100, 200 and 350, respectively
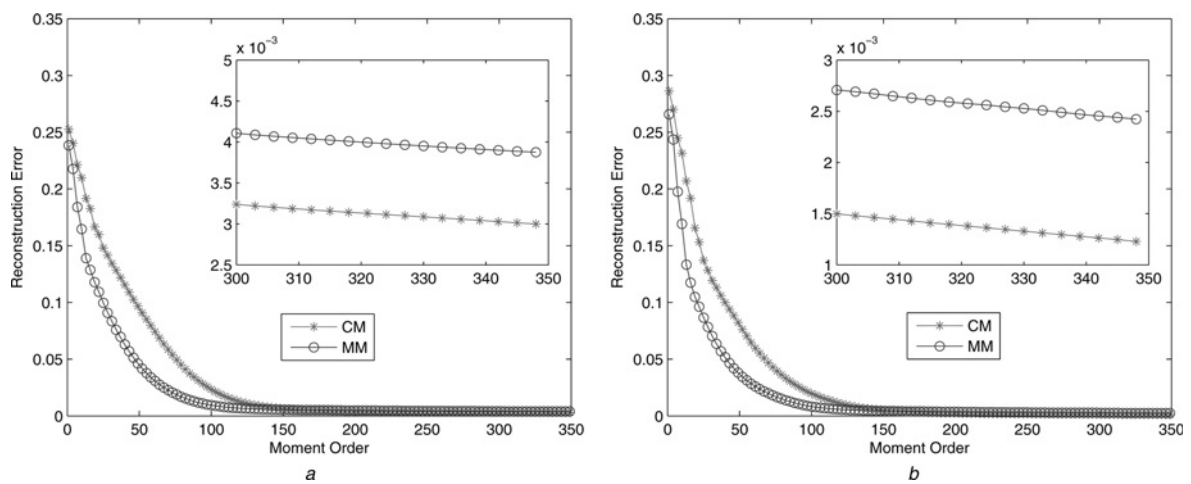
Figure 10 *Comparative study of reconstruction errors by using MM (($\beta_1 = \beta_2 = 110, \mu_1 = \mu_2 = 0.5$) and CM ($a_1 = a_2 = 128$) in two different images*

a Test image Hill
b Test image Sea
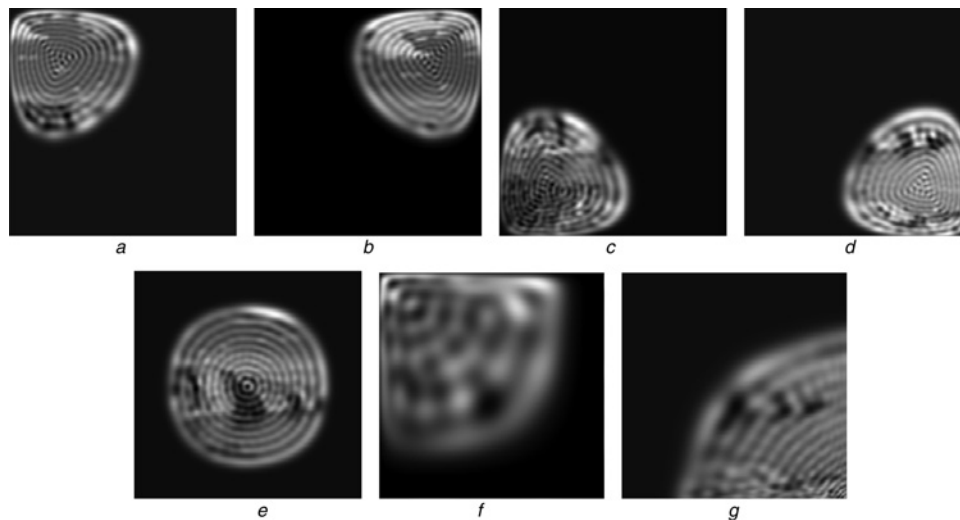
Figure 11 *Reconstructed images using different moments up to order 35*

a KM ($p_1 = p_2 = 0.1$)
b KM ($p_1 = 0.1, p_2 = 0.9$)
c KM ($p_1 = 0.9, p_2 = 0.1$)
d KM ($p_1 = p_2 = 0.9$)
e KM ($p_1 = p_2 = 0.5$)
f HM ($a_1 = a_2 = 100, b_1 = b_2 = 0$)
g HM ($a_1 = a_2 = 0, b_1 = b_2 = 100$)

orthogonal in an unlimited region, the moments' orders can be calculated as high as possible. In theory, higher the moment order is, better the reconstructed image. In Fig. 10, the mse still tends to decrease while the moment order is up to 350. However, it is impossible to calculate image moments without an edge or limit. Here, when to stop the reconstruction process is an open question. We will investigate it elsewhere.

5.5 Local feature extraction

From Fig. 1, it is examined that the value of polynomials' parameters will bring some influences on the emphasis region of these polynomials. This property can be used to extract the local information of images. In the following experiments, we will show how these moments can be utilised to capture the local information of an image, while
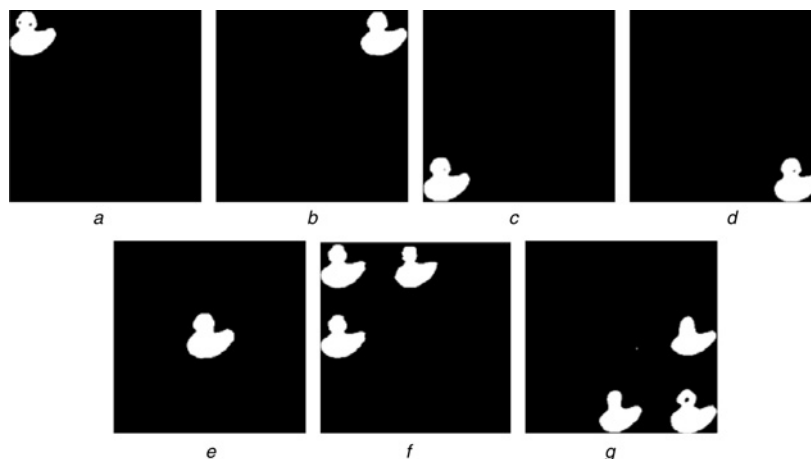
Figure 12 *Reconstructed images (thresholded) up to order 25*

a KM ($p_1 = p_2 = 0.1$)
b KM ($p_1 = 0.1, p_2 = 0.9$)
c KM ($p_1 = 0.9, p_2 = 0.1$)
d KM ($p_1 = p_2 = 0.9$)
e KM ($p_1 = p_2 = 0.5$)
f HM ($a_1 = a_2 = 100, b_1 = b_2 = 0$)
g HM ($a_1 = a_2 = 0, b_1 = b_2 = 100$)
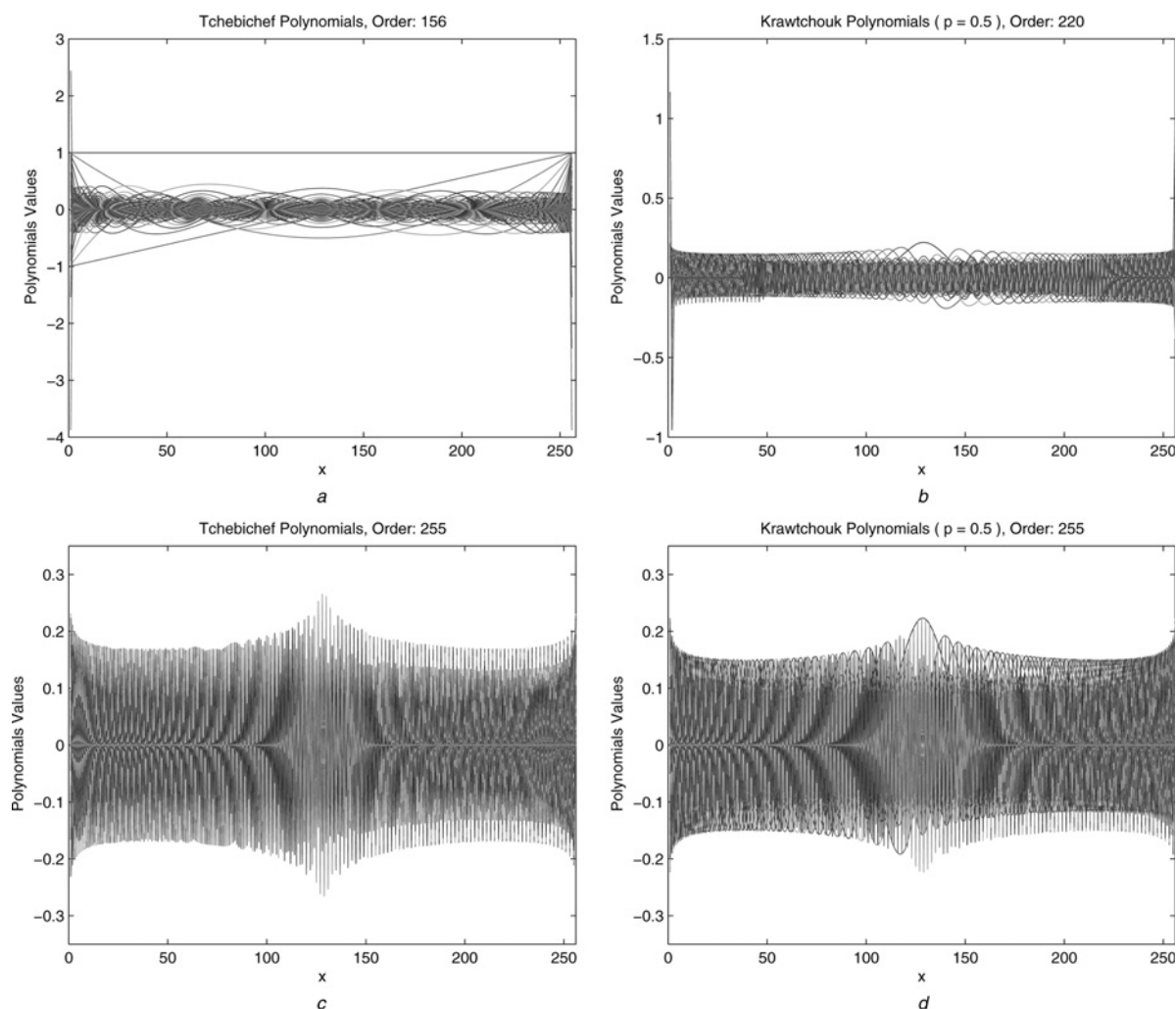
Figure 13 *Plots of normalised polynomials when N = 256*

a Tchebichef [6]
b Krawtchouk [7]
c, d Plots using the proposed general form (27)

the parameters p, a and b are set the local feature extraction mode. From Fig. 11, one can find that the local information of an image is emphasised at low orders, if parameters p, a and b are well set. This phenomenon is also verified by reconstructed images in Fig. 12.

5.6 Numerical stability of the general forms

In the final experiment, we demonstrate why the proposed general forms are important in theory and engineering. It is well known that the hypergeometric functions (11), (14), (17), (20) and (23) are not suitable for defining the moments because the value of polynomials grows as N_n. On the other hand, the traditional recurrence relations of polynomial evaluation can lead to numerical problems when the required moment order is large. A comparison plots between Tchebichef and Krawtchouk polynomials using traditional methods [6, 7] are presented in Figs. 13a and b, which indicates that the range of the polynomials' values expands

rapidly when the order of polynomials is above a certain value. This is because the recurrence relation proposed by [6, 7] continues to propagate numerical errors, eventually leading to the instability observed in Fig. 13. This phenomenon is much more obvious while polynomials order increases above 156 for Tchebichef (above 200 for Krawtchouk). This causes some numerical problems in the computation of moments and therefore affects the features extracted from moments. Fig. 14 presents a comparative study of reconstructed images by using the methods of [6, 7], and the proposed general form (27). From Fig. 14, it is found that the feature extract capabilities of Tchebichef moments do not seem to be affected when the moment order increases from 0 to 150. However, it is dominated by numerical errors, which bring severe deterioration for the quality of image reconstruction, as the maximum moment order is above 150. From Figs. 13c and d, it is noted that unlike the traditional methods, the Tchebichef and Krawtchouk polynomial values calculated through the proposed general form are constrained to the interval $[-0.3, 0.3]$, where the occurrences of numerical

Figure 14 *Comparative study of reconstructed images by using the traditional methods and the proposed general form (27)* *(p₁ = p₂ = 0.5 for Krawtchouk moments)* *[6, 7]*

instabilities are eliminated when the polynomial order becomes large, so that very accurate results can be obtained while computing high-order moments and reconstructing images from the moments (see Fig. 14).

In [16], Mukundan realised this problem and introduced an effective method to compute Tchebichef polynomials by modifying the recurrence relation. In their work, the recurrence relation with respect to x rather than n was used to avoid cumulative multiplication of large values. Actually, the approach in [16] can be obtained from the proposed general form (27). In the current study, the proposed general form (27) is very effective in avoiding the numerical fluctuation in polynomials or moment computations. It can be used to calculate the high-order moments and to extract the features of an image in a large size.

On the other hand, the recurrence relation with respect to n (the traditional method) of all classical discrete orthogonal polynomials (including Tchebichef, Krawtchouk, Hahn, Meixner, Charlier, dual Hahn, Racah, q-analogues of the Hahn, Meixner, Krawtchouk, Charlier polynomials, etc.) can be deduced from the proposed general form (9).

6   Conclusions

In this paper, we have presented two general forms for computing discrete orthogonal polynomials and their corresponding discrete orthogonal moments. The importance of the proposed general forms in application has been analysed. Some useful properties of these general forms have been discussed. These properties can be used to compress a natural image, as well as reconstruct an image with a large size. Owing to the influence of the parameters on orthogonal polynomials, an image's global and local information can be emphasised by choosing right values for the parameters. Thus, one can make local feature extraction more flexible by modifying particular parameters of polynomials, such as Krawtchouk and Hahn polynomials.

Owing to the limit of the space, this study omits the discussion of choosing parameters for the proposed orthogonal polynomials. However, the proposed methods and general forms can be easily extended to obtain other orthogonal polynomials and their corresponding moments. Further work in the field of these discrete orthogonal moments is directed towards the identification of invariants.

7   Acknowledgments

8   References

[1]   HADDADNIA J., AHMADI M., FAEZ K.: 'An efficient feature extraction method with pseudo-Zernike moment in RBF neural network-based human face recognition system', *EURASIP J. Applied Signal Process.*, 2003, **1**, pp. 890–901

[2]   KAMILA N.K., MAHAPATRA S., NANDA S.: 'Invariance image analysis using modified Zernike moments', *Pattern Recogn. Lett.*, 2005, **28**, pp. 747–753

[3]   TEAGUE M.R.: 'Image analysis via the general theory of moments', *J. Opt. Soc. Am.*, 1980, **70**, pp. 920–930

[4]   TEH C.H., CHIN R.T.: 'On image analysis by the method of moments', *IEEE Trans. Pattern Anal. Mach. Intell.*, 1988, **10**, pp. 496–513

[5]   MUKUNDAN R., ONG S.H., LEE P.A.: 'Discrete vs. continuous orthogonal moments for image analysis'. Int. Conf. on Imaging Science, Systems and Technology-CISST'01, 2001, pp. 23–29

[6]   MUKUNDAN R., ONG S.H., LEE P.A.: 'Image analysis by Tchebichef moments', *IEEE Trans. Image Process.*, 2001, **10**, pp. 1357–1364

[7]   YAP P.-T., PARAMESRAN R., ONG S.-H.: 'Image analysis by Krawtchouk moments', *IEEE Trans. Image Process.*, 2003, **12**, pp. 1367–1377

[8]   ZHOU J., SHU H., ZHU H., TOUMOULIN C., LUO L.: 'Image analysis by discrete orthogonal Hahn moments'. Proc. Second Int Conf. Image Analysis and Recognition, 2005, pp. 524–531

[9]   ZHU H., SHU H., ZHOU J., LUO L., COATRIEUX J.L.: 'Image analysis by discrete orthogonal dual-Hahn moments', *Pattern Recogn. Lett.*, 2007, **28**, pp. 1688–1704

[10] ZHU H., SHU H., LIANG J., LUO L., COATRIEUX J.L.: 'Image analysis by discrete orthogonal Racah moments', *Signal Process.*, 2007, **87**, pp. 687–708

[11] NIKIFOROV A.F., UVAROV V.B.: 'Special functions of mathematical physics' (Birkhauser, Bessel, Boston, 1988)

[12] NIKIFOROV A.F., SUSLOV S.K., UVAROV V.B.: 'Classical orthogonal polynomials of a discrete variable' (Springer, New York, 1991)

[13] KOEKOEK R., SWARTTOUW R.F.: 'The Askey-scheme of hypergeometric orthogonal polynomials and its q-analogue'. Report 98–17, Faculty of Technical Mathematics Informatics, Delft University of Technology, Delft, 1998

[14] YAP P.-T., PARAMESRAN R., ONG S.-H.: 'Image analysis using Hahn moments', *IEEE Trans. Pattern Anal. Mach. Intell.*, 2007, **29**, pp. 2057–2062

[15] KOEPF W., SCHMERASU D.: 'Representations of orthogonal polynomials', *J. Comput. Appl. Math.*, 1998, **90**, pp. 57–94

[16] MUKUNDAN R.: 'Some computational aspects of discrete orthogonal moments', *IEEE Trans. Image Process.*, 2004, **13**, pp. 1055–1059

[17] JAIN A.K.: 'Fundamentals of digital image processing' (Prentice-Hall, New Jersey, 1989)

[18] VILLASENOR J.D.: 'Alternatives to discrete cosine transform for irreversible tomographic image compression', *IEEE Trans. Med. Imag.*, 1993, **12**, pp. 803–811

[19] HAMIDI M., PEARL J.: 'Comparison of cosine and Fourier transforms of Markov-l signals', *IEEE Trans. ASSP.*, 1976, **24**, pp. 428–429